Solution Structure and Functional Characterization of Jingzhaotoxin-XI: A Novel Gating Modifier of both Potassium and Sodium Channels[†,‡]

Zhi Liao,[§,||] Chunhua Yuan,[§,⊥] Meichun Deng,[⊥] Jiang Li,[⊥] Jinjun Chen,[⊥] Yuejun Yang,[⊥] Weijun Hu,[⊥] and Songping Liang*[,⊥]

College of Life Sciences, Peking University, Beijing 100083, China, and The Key Laboratory of Protein Chemistry and Developmental Biology of Ministry of Education, College of Life Sciences, Hunan Normal University, Changsha 410081, China

Received July 19, 2006; Revised Manuscript Received September 26, 2006

ABSTRACT: JZTX-XI is a peptide toxin isolated from the venom of the Chinese spider *Chilobrachys jingzhao*. It contains 34 residues including six cysteine residues with disulfide bridges linked in the pattern of I−IV, II−V, and III−VI. Using 3′- and 5′-RACE methods, the full-length cDNA was identified as encoding an 86-residue precursor of JZTX-XI. In the electrophysiological assay, JZTX-XI shows activity toward the Kv2.1 channel in a way similar to hanatoxin1 and SGTx1 that both the activation and the deactivation processes are affected, which is in accordance with the high sequence homology among them (over 60% identity). On the other hand, JZTX-XI also exhibits specific interaction against the Nav channels of rat cardiac myocytes with a significant reduction in the peak current and slowing of channel inactivation. The solution structure of native JZTX-XI was determined by ^{1}H NMR methods to identify the structural basis of these specific activities. Structural comparison of JZTX-XI with other gating modifier toxins shows that they all adopt a similar surface profile, a hydrophobic patch surrounded by charged residues such as Arg or Lys, which might be a common structural factor responsible for toxin−channel interaction. JZTX-XI might be an ideal tool to further investigate how spider toxins recognize various ion channels as their targets.

Voltage-gated ion channels are transmembrane proteins and play crucial roles in a wide range of physiological processes. These channels are generally composed of two types of functional domains: the central pore domain constructed from the tetrameric arrangement of the S5−S6 segments and the voltage-sensing domains constructed from the S3−S4 segments (*1*−*5*). The mechanism and physiological role of some ion channels are now better understand thanks to the discovery of animal toxins that bind with high affinity and specificity to the different ion channels.

Spider venoms contain abundant peptide toxins that target various voltage-gated ion channels, and many of them are invaluable tools for elucidating the physiological properties of these ion channels. Some of these peptide toxins, such as hainantoxin-I and hainantoxin-IV, might block voltage-gated sodium channels by occluding the channel pore to block the flow of ions (*6*, *7*). On the other hand, gating modifier toxins, such as hanatoxin1 and ω-agatoxin-IVA, inhibit ion channels by binding to the voltage-sensing domains and affecting the voltage-dependent gating process (*8*, *9*). Determination of spatial structures of these toxins has provided a foundation for investigating the molecular basis of toxin specificity and for drug development directed against ion channel related diseases.

JZTX-XI[1] is a novel spider toxin purified from the venom of the Chinese tarantula *Chilobrachys jingzhao*, with 34 residues and stabilized by three disulfide bridges. This toxin shares high sequence similarity with several well-characterized spider toxins that act on diverse voltage-gated ion channels. The cDNA sequence of JZTX-XI was determined by RACE methods. Electrophysiological investigations on JZTX-XI were performed via the voltage clamp method on Kv1, Kv2, Kv3, and Kv4 subtypes expressed in *Xenopus laevis*. JZTX-XI's activity on Nav and Cav channels was tested by whole-cell patch-clamp techniques on rat DRG neurons and cardiac myocytes. JZTX-XI's solution structure was determined by ^{1}H 2D NMR methods. Structural comparison and sequence alignment among JZTX-XI and other toxins acting on Kv channels or Nav channels show some significant clues for JZTX-XI's structure−function relationship against the Kv2.1 channel or Nav channel.

[†] This work was supported by grants from National Natural Science Foundation of China (under Contract 30430170).

[‡] The atomic coordinates and structure factors (code 2A2V, native JZTX-XI) have been deposited in the Protein Data Bank, Research Collaboratory for Structural Bioinformatics, Rutgers University, New Brunswick, NJ (http://www.rcsb.org/).

* Corresponding author. Tel: 86-731-8861304. Fax: 86-731-8861304. E-mail: liangsp@hunnu.edu.cn.

[§] Equal contribution to this work.

[||] Peking University.

[⊥] Hunan Normal University.

[1] Abbreviations: JZTX, jingzhaotoxin; δ-ACTX, δ-atracotoxin; TTX, tetrodotoxin; CCA, α-cyano-4-hydroxycinnamic acid; TFA, trifluoroacetic acid; HEPES, *N*-(2-hydroxyethyl)piperazine-*N*′-2-ethanesulfonic acid; DRG, dorsal root ganglion; RACE, rapid amplification of cDNA ends; HPLC, high-pressure liquid chromatography; MALDI-TOF, matrix-assisted laser desorption/ionization time of flight; NMR, nuclear magnetic resonance; NOE, nuclear Overhauser effect; DQF-COSY, double-quantum-filtered correlation spectroscopy; TOCSY, total correlated spectroscopy; NOESY, nuclear Overhauser effect spectroscopy; rms, root mean square.

10.1021/bi061457+ CCC: $33.50
Published on Web 12/19/2006

Here, we report the purification, electrophysiological characterization, cDNA sequence, and solution structure of JZTX-XI.

MATERIALS AND METHODS

Materials and Animals. Sprague-Dawley rats were purchased from Xiangya School of Medicine, Central South University. Cockroaches were from our laboratory stock colonies. All sequencing reagents were purchased from Applied Biosystems (Foster City, CA), Division of Perkin-Elmer. The 3′- and 5′-RACE kits and Trizol reagent were purchased from Invitrogen Inc. Restriction enzymes, Taq DNA polymerase, and the pGEMT easy vector system were from Promega. TFA and CCA were from Sigma. All other reagents are of analytical grade.

Purification of JZTX-XI. The venom from the female Chinese tarantula spider *C. jingzhao* was collected as described in our previous work (*10*). The freeze-dried crude venom was stored at −20 °C prior to analysis. Lyophilized crude venom was suspended in distilled water, centrifuged (2000*g*, 4 °C, 10 min), filtered on 0.45 μm microfilters, and then loaded onto a Waters Protein-Pak CM 8H column (5 × 50 mm) initially equilibrated with 0.1 M sodium phosphate buffer, pH 6.25 (buffer A). The column was eluted with a linear gradient of 5−60% buffer B (1.0 M sodium chloride, 0.1 M sodium phosphate, pH 6.25) over 45 min at a flow rate of 2.0 mL/min. The fraction of interest was collected and applied onto a reverse-phase RP-HPLC column (Vydac C18, 300 Å, 4.6 × 250 mm) using a Waters Alliance system. Venom components were eluted using a linear acetonitrile gradient (5−45% acetonitrile/0.1% TFA in 55 min) at a flow rate of 1.0 mL/min. Elution of peptides was monitored at 280 nm.

Mass Spectrometry. The molecular mass of peptides was determined using MALDI-TOF MS (Applied Biosystems, Voyager-DE STR biospectometry workstation). Ionization was achieved by irradiation with a nitrogen laser (337 nm), with a 20 k*V* acceleration voltage. CCA was used as the matrix.

Amino Acid Sequencing by Automated Edman Degradation. The native peptide was submitted to automatic N-terminal sequencing on an Applied Biosystems Model 491 gas-phase sequencer. Edman degradation was performed with a normal automatic cycle program.

Isolation and Characterization of JZTX-XI cDNA. The full length of JZTX-XI cDNA was obtained using 3′- and 5′-RACE methods as described previously (*10*). First, according to the manufacturer's instructions, the total RNA was extracted from 0.1 g of fresh venom glands of female spiders using the TRIzol reagent kit. Five micrograms of RNA was taken to convert mRNA into cDNA using the Superscript II reverse transcriptase with an universal oligo(dT)-containing adapter primer [5′-GGCCACGCGTCGACTAGTAC$(dT)_{17}$-3′]. The cDNA was then used as template for PCR amplification in 3′-RACE. A degenerate primer 1 [5′-CA-(C/T)(C/T)T(T/C/G/A)GG(T/C/G/A)TG(T/C)AA(G/A)CC-(T/C/G/A) AC-3′] was designed corresponding to the N-terminal residues ($_{18}$HLGCKPT$_{25}$) of mature JZTX-XI. The partial cDNA of mature toxin was amplified by the PCR technique using primer 1. Second, on the basis of the partial cDNA sequence of JZTX-XI determined by 3′-RACE, the antisense primers were designed and synthesized for 5′-RACE as follows: the gene-specific primer 2 (5′-TCCATC-CCATGCACAATATTT-3′). With the strategy described by the RACE kit supplier, the 5′-end cDNA of JZTX-XI was amplified using its gene-specific primer 2. Amplified products in both 3′- and 5′-RACE were precipitated and cloned into the pGEM-T easy vector for sequencing. DNA sequencing was performed by Bioasia Inc. Nucleic acid sequences were analyzed using the software of DNAclub (by Xiongfong Chen, www.imtech.res.in/pub/nsa/dnaclub/dos/) and DNAman (by Nynnon biosoft, www.Lynnon.com).

Biological Assays. The toxicity of JZTX-XI was qualitatively assayed by intraperitoneal injection into 18−20 g mice of both sexes and intraabdominal injection into adult male cockroaches (*Periplaneta americana*) with body weights of 0.3−0.5 g using 20 μL solutions [in 0.9% (w/v) normal saline].

Two-Microelectrode Voltage Clamp Experiments. Capped cRNAs encoding ion channels were synthesized after linearizing the plasmids and performing the transcription by a standard protocol (*11*). For in vitro transcription, the plasmids pCI containing the genes for Kv2.1, Kv4.1, and Kv1.1 were first linearized with *Not*I, respectively; the plasmid PcDNA3.1 containing the gene for Kv4.2 was linearized with *Sma*I; the plasmid PcDNA3 containing the gene for Kv1.2 was linearized with *Sph*I; the plasmid pCI-neo containing the gene for Kv1.3 was linearized with *Not*I; the plasmids pSP64 containing the genes for Kv1.4 and Kv3.1 were linearized with *Eco*RI. Using the linearlized plasmids as templates, cRNAs were synthesized in vitro using the large-scale T7, SP6, or T3 mMESSAGE mMACHINE transcription kit (Ambion).

Stage V−VI *X. laevis* oocytes were collected from mature female *X. laevis* under anesthesia by putting on ice. Then the oocytes were defolliculated by treatment with 1 mg/mL collagenase in calcium-free ND96 solution (pH 7.5) containing (in mM) 96 NaCl, 2 KCl, 1 $MgCl_2$, and 10 HEPES. Between 2 and 24 h after defolliculation, oocytes were injected with 41 nL of 100−500 ng/μL cRNA using a Microprocessor controlled nanoliter injector (WPI). The oocytes were then incubated in OR_2 solution (pH 7.5) at 18 °C for 1−4 days. OR_2 solution contains (in mM) 82.5 NaCl, 2.5 KCl, 1 $CaCl_2$, 1 Na_2HPO_4, 1 $MgCl_2$, and 5 HEPES, supplemented with 50 mg/L gentamycin sulfate (only for incubation).

Whole-cell currents from oocytes were recorded using the two-microelectrode voltage clamp (TURBO TEC-03X; NPI Electronic). Voltage and current electrodes (0.1−0.8 MΩ) were filled with 3 M KCl. Oocytes were studied in a 100 μL recording chamber that was perfused with an extracellular solution containing RbCl (50 mM), NaCl (50 mM), $MgCl_2$ (1 mM), $CaCl_2$ (0.3 mM), and HEPES (5 mM), pH 7.5, with NaOH. Current records were sampled at 0.5 ms intervals after low-pass filtering at 2 kHz. Linear components of capacity and leak currents were not subtracted. All experiments were performed at room temperature (19−23 °C).

Whole-Cell Patch-Clamp Experiments. Acutely dissociated DRG cells were prepared from 4-week-old Sprague-Dawley rats and maintained in short-term primary culture using the method described in previous work (*12*). The dissociated cells were suspended in essential DMEM medium supplemented with 10% fetal bovine serum, 50 IU/mL penicillin, and 50

μg/mL streptomycin. The cells were plated on a poly(L-lysine)-coated dish (35 × 10 mm) and incubated at 37 °C in an atmosphere of 5% CO_2. Cells in culture for 3−24 h were used in the patch experiments. Experiments were conducted at room temperature (20−25 °C). Single ventricular cardiomyocytes were enzymatically dissociated from adult rats by a previously described method (*13*). Whole-cell cardiac sodium currents were recorded from rod-shaped cells with clear cross-striations at room temperature (20−25 °C).

Cell current recordings were made with the whole-cell patch-clamp technique using an EPC-9 patch-clamp amplifier (HEKA Electronid, Lambrecht, Germany). Voltage steps and data acquisition were controlled using a PC computer with the software Pulsefit+Pulse 8.0 (HEKA Electronid, Lambrecht, Germany). The patch pipets with DC resistances of 2−3 MΩ were fabricated from borosilicate glass tubing (VWR micropipets, 100 μL; VWR Co.) using a two-stage vertical microelectrode puller (PC-10, Narishige, Japan) and fire-polished by a heater (Narishige, Japan). Data were sampled at 10 kHz and filtered at 3 kHz. Under voltage clamp 70−80% series resistance compensation was applied.

Ca^{2+} channel currents (I_{Ca}) were measured using Ba^{2+} as a charge carrier (I_{Ba}). For Ca^{2+} current recordings, the external solution contained (in mM) 160 TEA-Cl, 10 HEPES, 2 $BaCl_2$, 10 D-glucoses, and 200 nM TTX, adjusted to pH 7.4 with TEA-OH. The internal solution contained (in mM) 120 $CsCl_2$, 5 MgATP, 0.4 Na_2GTP, 10 EGTA, and 20 HEPES−CsOH at pH 7.2. $I_{Ba}{}^{2+}$ was evoked at −50 or 0 mV from a holding potential of −90 or −40 mV.

For Na^+ current recordings, the bath solution contained (in mM) 150 NaCl, 2 KCl, 5 D-glucose, 1 $MgCl_2$, 1.5 $CaCl_2$, and 10 HEPES at pH 7.4; the pipet internal solution contained (in mM) 105 CsF, 35 NaCl, 10 HEPES, and 10 EGTA at pH 7.4. Sodium currents were elicited by depolarization from −80 to +50 mV from a holding potential of −80 mV.

NMR Spectroscopy. The NMR sample was prepared by dissolving the native JZTX-XI in 500 μL of 20 mM deuterium sodium acetate buffer (H_2O/D_2O, 9:1 v/v) containing 0.002% NaN_3 and 0.01 mM EDTA with a final concentration of 6 mM JZTX-XI and a pH of 4.0. Sodium 3-(trimethylsilyl)propionate-2,2,3,3-d_4 was added to a final concentration of 200 μM as an internal chemical shift reference. For experiments in D_2O, the sample used in H_2O experiments was lyophilized and then redissolved in 500 μL of 99.996% D_2O (Cambridge Isotope Laboratories). All NMR spectra were observed on a 500 MHz Bruker DRX-500 spectrometer with a sample temperature of 298 K. Several sets of two-dimensional spectra were recorded in a phase-sensitive mode by the time-proportional phase increment method following standard pulse sequences and phase cycling. TOCSY spectra were obtained with a mixing time of 85 ms. NOESY spectra were recorded in D_2O with a mixing time of 200 ms and in H_2O with mixing times of 100, 200, and 400 ms. Solvent suppression was achieved by the presaturation method. All two-dimensional measurements were recorded with 1024−512 frequency data points and were zero-filled to yield 2048−1024 data matrices except for the high-resolution DQF-COSY spectrum. The DQF-COSY spectrum was recorded with 2048−1024 data points in the t_2 and t_1 dimensions, respectively, and zero-filled to 4096−2048 points to measure the coupling constants. All spectra were processed and analyzed using Felix 98.0 (Biosym Technologies) software running on a Silicon Graphics O2 workstation. Before Fourier transformation, the signal was multiplied by a sine bell or sine bell square window functions with a $\pi/2$ phase shift.

Structure Calculations. Distance constraints were obtained from the intensities of cross-peaks in NOESY spectra with a mixing time of 200 ms. All NOE data were classified into four distance ranges: 1.8−2.7, 1.8−3.5, 1.8−5.0, and 1.8−6.0 Å, corresponding to strong, medium, weak, and very weak NOE values, respectively. Pseudoatom corrections were applied to nonstereospecifically assigned methyl and methylene protons according to the method of Wüthrich (*14*). Six dihedral angle restraints derived from $^3J_{NH-C\alpha H}$ coupling constants were restrained to $-120 \pm 30°$ for $^3J_{NH-C\alpha H} \geq 8.80$ Hz and $-65 \pm 25°$ for $^3J_{NH-C\alpha H} \leq 5.5$ Hz. Three distance constraints were added to every disulfide bridge that was mainly determined from NMR data. The corresponding distances were 2.02 ± 0.02, 2.99 ± 0.5, and 2.99 ± 0.5 Å for S(i)−S(j), S(i)−Cβ(j), and S(j)−Cβ(i), respectively. Structure calculations of JZTX-XI were run on a Silicon Graphics workstation using the standard protocol of the X-PLOR-NIH-2.9.6 program (*15*).

RESULTS

Purification and Sequence Analysis of JZTX-XI. Crude venom from the spider *C. jingzhao* was fractionated by ion-change HPLC on a Waters Protein-Pak CM 8H column (Figure 1A). About eight peaks were eluted in the chromatogram. The fraction labeled with the asterisk was collected and further purified by RP-HPLC on a Vydac C18 column (Figure 1B). The peak labeled JZTX-XI, which eluted at 14 min with the gradient of about 30% acetonitrile, was further purified by an analytic RP-HPLC (Figure 1B, inset). The purity of JZTX-XI was over 99%, as judged by RP-HPLC and N-terminal sequencing. The complete amino acid sequence of JZTX-XI was derived by Edman degradation, revealing that it is a 34 amino acid polypeptide containing six cysteine residues. The molecular mass of JZTX-XI measured by MALDI-TOF mass spectrometry (3726.38 Da) is −1 Da different from the molecular mass calculated with a carboxylic C-terminus (3727.32 Da), which indicates amidation at the C-terminus of JZTX-XI, in accordance with the cDNA sequence of JZTX-XI (Figure 2B). Online BLAST search (www.ncbi.nlm.nih.gov/blast) showed that JZTX-XI has high sequence identity with several spider toxins identified as Kv, Cav, and Nav channel modifiers (stromatoxin-1, 73%; heteroscodratoxin-1, 70%; hanatoxin1, 70%; SGTx1, 64%; SNX-482, 64%; toxin CcoTx3, 58%; shown in Figure 2A). The sequential similarities among them might be therefore substantial clues for investigating the bioactivity of JZTX-XI against various ion channels.

Cloning and Sequencing JZTX-XI cDNA. The full-length cDNA sequence of JZTX-XI was completed by overlaying two fragments resulting from 3′- and 5′-RACE. As shown in Figure 2B, the oligonucleotide sequence of the cDNA was a 468 bp bond found to comprise the 5′-untranslated region (UTR), open reading frame, and 3′-UTR. The open reading frame encoded a 86-residue peptide corresponding to the JZTX-XI precursor which contained a signal peptide of 21

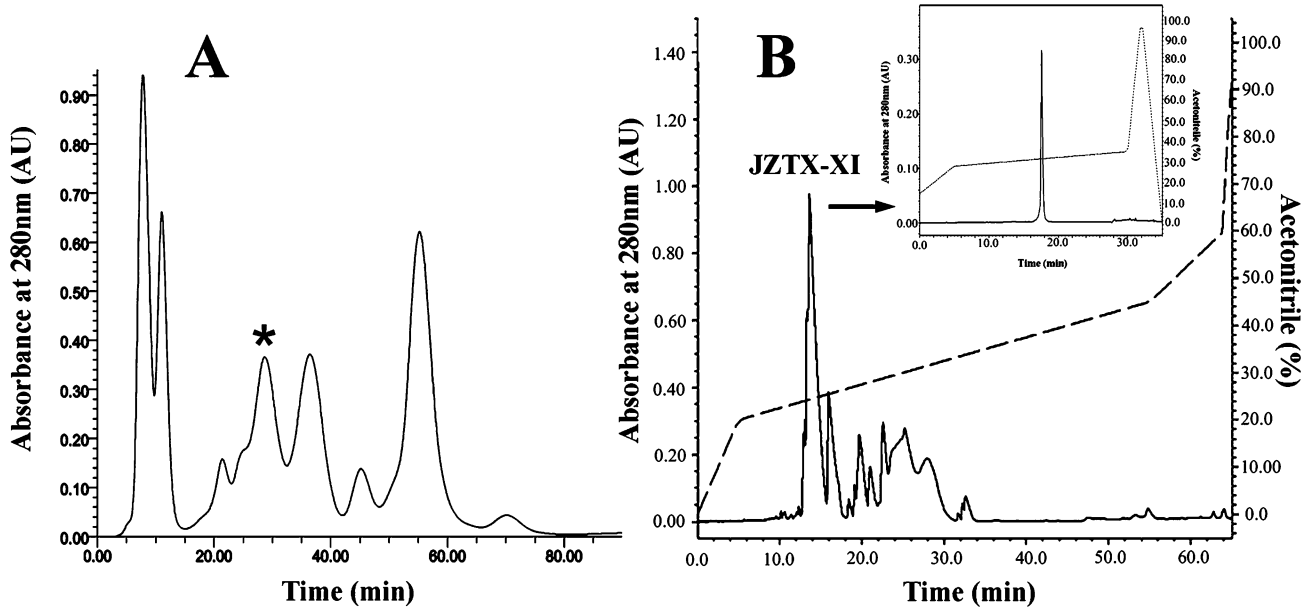

FIGURE 1: Purification and identification of JZTX-XI. (A) Ion-exchange HPLC chromatograph of the crude venom from the Chinese spider *C. jingzhao*. The peptides were eluted with a linear gradient of 5−60% buffer (1.0 M sodium chloride, 0.1 M sodium phosphate, pH 6.25) over 45 min at a flow rate of 2.0 mL/min. The asterisk indicates the fraction of interest with a retention time of 29.5 min. (B) Reverse-phase HPLC profile of the fraction of interest on a Vydac C18 column (4.6 mm × 250 mm). The peptide was eluted with a linear gradient of 5−45% acetonitrile/0.1% TFA for 55 min at a flow rate of 1.0 mL/min. The inset shows further purification of JZTX-XI on analytical RP-HPLC yielding a single peak.

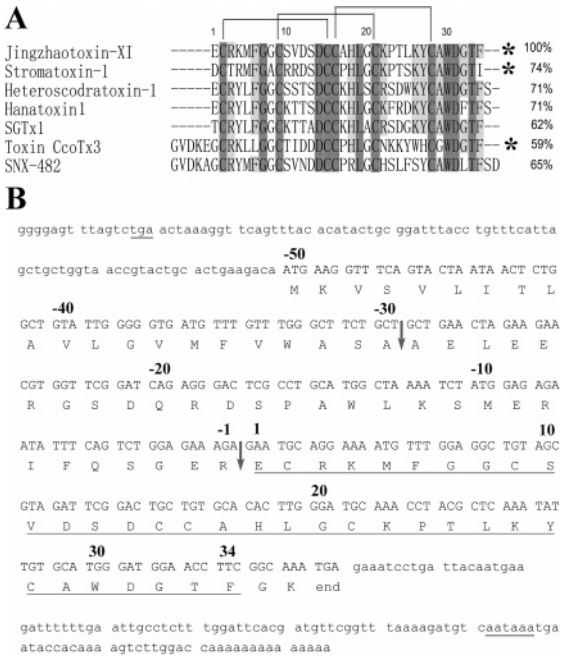

FIGURE 2: Amino acid sequence and cDNA sequence of JZTX-XI. (A) Sequence alignment of JZTX-XI with some other toxins. Identical amino acids are shown in gray, and the well-conserved residues are in black. The percentage identity (%) is shown to the right of the sequences. The disulfide linkage is indicated above as lines. An asterisk indicates the amidation at the C-terminal carboxyl group. (B) The oligonucleotide sequence of JZTX-XI cDNA. The amino acid composition of the precursor reading from the cDNA is suggested below the nucleotide sequence. The potential endoproteolytic sites are indicated with down arrows. The sequence of the mature peptide is underlined.

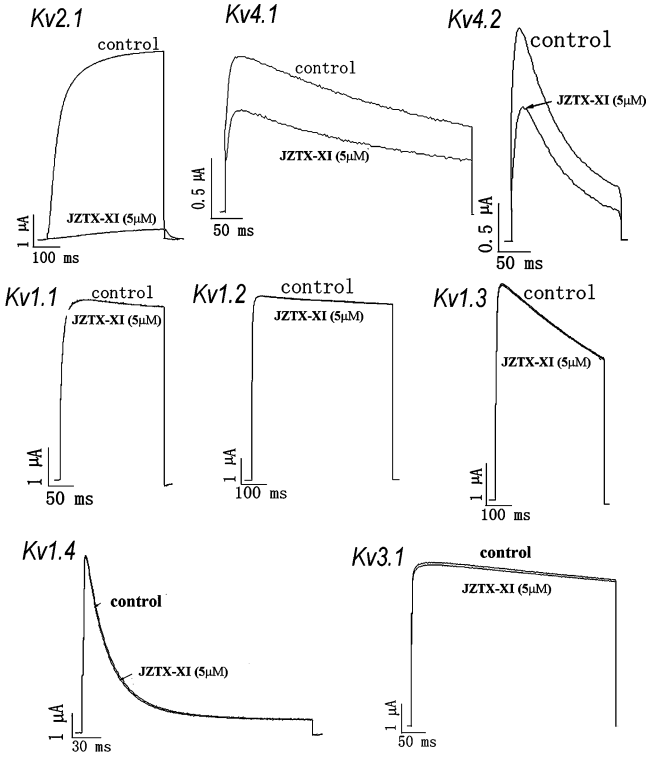

FIGURE 3: Effects of 5 μM JZTX-XI on various Kv channel subtypes. All channels were expressed in *Xenopus* oocytes by injection of cDNA. For Kv1.4, Kv4.1, and Kv4.2, current traces were evoked by a 200 ms depolarization to +20 mV from a holding potential of −90 mV. For Kv1.1, Kv1.2, and Kv1.3, currents were elicited by a 400 ms depolarization to +20 mV from a holding potential of −80 mV. For Kv2.1 and Kv3.1, current traces were evoked by a 300 ms depolarization to 0 mV from a holding potential of −80 mV.

residues, a propeptide of 29 residues, a mature peptide of 34 residues, and 2 extra residues (-Gly-Lys) at the C-terminus (Figure 2). The signal peptide sequence of the JZTX-XI includes a hydrophobic core rich in Val and Leu and a consensus cleavage point for a signal peptidase. The intervening propeptide region of this toxin is rich in Glu residues and contains a common endoproteolytic site (-X-Arg-). The

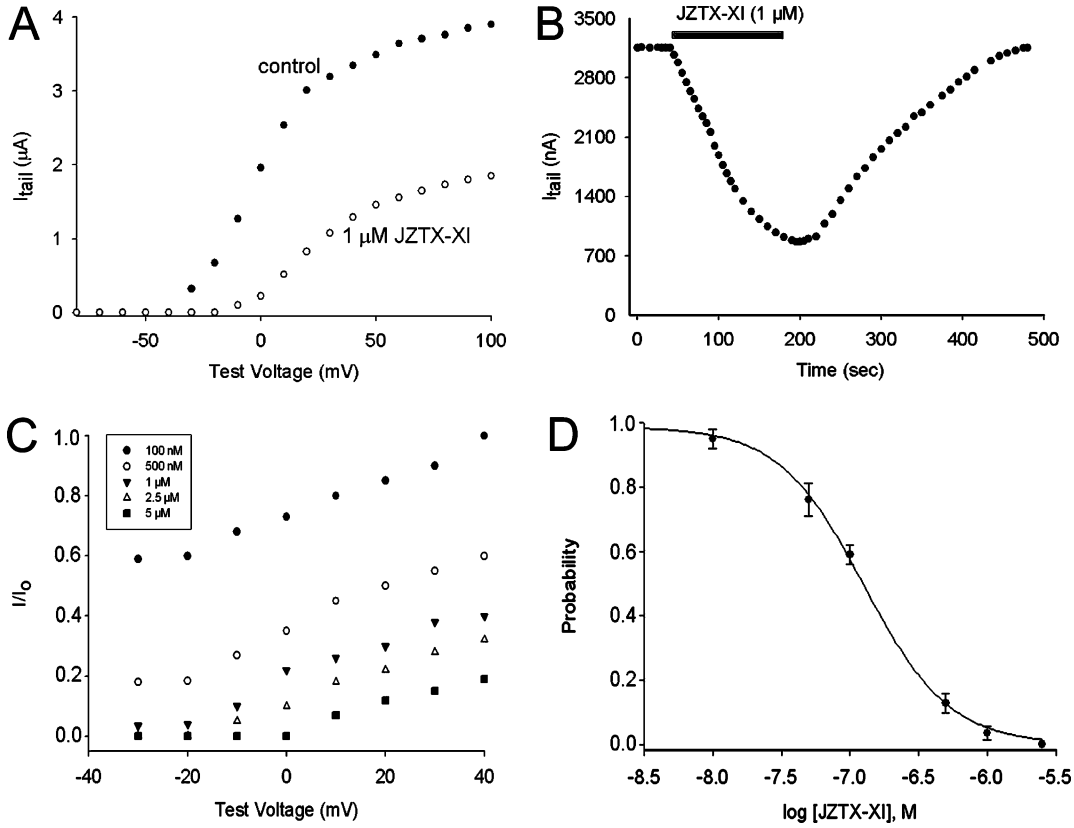

FIGURE 4: Inhibition of the Kv2.1 currents by JZTX-XI. (A) Voltage−activation relations in the absence and presence of 1 μM JZTX-XI. Current traces were evoked by a 300 ms depolarization to various test potentials from a holding potential of −80 mV. Tail current amplitude measured at −50 mV was plotted as a function of the preceding test depolarization in either the absence or presence of 1 μM JZTX-XI. Tail current amplitude was averaged for 0.5 ms beginning 3 ms after repolarization to −50 mV. (B) Time course for inhibition of the Kv2.1 channel by 1 μM JZTX-XI. Currents were elicited by depolarization to 0 mV from a holding potential of −80 mV and a tail voltage of −50 mV. (C) Fraction of uninhibited tail currents in the presence of various concentrations of JZTX-XI. Currents were elicited by various strength depolarizations from a holding potential of −80 mV and a tail voltage of −50 m*V*. *I* and I_0 represent the tail currents in the presence and absence of JZTX-XI, respectively, measured 3 ms after repolarization to −50 mV and averaged over 0.5 ms. (D) Concentration dependence for fractional occupancy of the Kv2.1 channel by JZTX-XI. Plot of fraction unbound for varying concentrations of JZTX-XI. The fraction of uninhibited tail current was measured in the plateau phase of the relations typically following depolarization between −30 and −20 mV. Data points are the mean ± SEM for five to seven cells at each concentration of toxin. The solid line is a fit of the data to $\rho_0 = (1 - \rho)^4$, where ρ_0 is the probability of the channel having zero JZTX-XI bound and ρ = [JZTX-XI]/([JZTX-XI] + K_d) with K_d = 0.74 μM. This equation assumes four equivalent and independent binding sites.

2 extra amino acid residues GK at its C-terminus are known to allow "postmodification" α-amidation at the C-terminal residue (*16*), which implies that the C-terminal residue of mature toxin is amidated. A polyadenylation signal (AATAAA) emerged in the 3′-UTR at position 24 upstream of the poly-(A).

Biological Assays. JZTX-XI was assayed in vivo by direct injection into mice and cockroaches. It showed no significant toxic symptoms in them during a period of 48 h postinjection.

Effect of JZTX-XI on Kv Channels. Figure 3 shows the effect of JZTX-XI on various Kv channel subtypes expressed in *Xenopus* oocytes. JZTX-XI (5 μM) had no significant effect on Kv1.1, Kv1.2, Kv1.3, Kv1.4, and Kv3.1 currents, whereas it reduced Kv2.1, Kv4.1, and Kv4.2 currents by ∼95%, ∼35%, and ∼42%, respectively (Figure 3). When JZTX-XI (1 μM) is applied to the extracellular solution, it shifts the activation of the Kv2.1 channel to more depolarized voltages (Figure 4A), similar to that previously observed for hanatoxin1. Kinetic studies for JZTX-XI-induced inhibition of the Kv2.1 channel are shown in Figure 4B. At a concentration of 1 μM, the toxin produces about 75% inhibition with the time constant of 126 s. The voltage-activated currents recover to control levels after removal of the toxin from the recording chamber with the time constant of 213 s. In contrast to pore-blocking toxins, the JZTX-XI's kinetics of onset of inhibition and recovery from inhibition is slower, which is similar to hanatoxin1 or other gating modifier toxins. The slow inhibition kinetics of the toxin may be related to the rate of membrane partitioning or efficiency of successful encounter in the toxin channel binding step or by a combination of both effects according to the previous work by Seok-Yong Lee et al. (*17*). We determined the equilibrium dissociation constant (K_d) for JZTX-XI binding to the Kv2.1 channel by measuring the concentration dependence for toxin occupancy of the channels as previously described for hanatoxin1 (*18*). Figure 4C shows the concentration dependence for fractional inhibition of tail currents for various strength depolarizations. At negative voltages, the fraction of uninhibited tail current reaches a plateau. This suggests that when even a single JZTX-XI molecule binds to a channel, the bound channels will not open at these voltages. On the basis of the results, the K_d (0.74 μM) was determined by measuring the fraction of uninhibited current at negative test voltages (where this quantity represents the fraction of unbound channels) (Figure 4D).

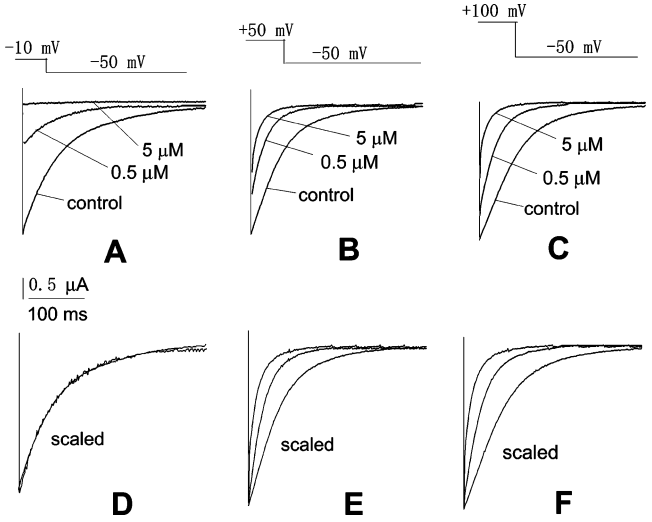

FIGURE 5: Tail currents elicited following various strength depolarizations in different concentrations of JZTX-XI. (A−C) Tail currents elicited at −50 mV following depolarization to −10, +50, and +100 mV in the absence or presence of 0.5 and 5 μM JZTX-XI. (D−F) Scaled records for two concentrations of the toxin for depolarizations to +50 and +100 mV and one concentration of the toxin for depolarization to −10 mV. JZTX-XI completely inhibits the opening of channels at the concentration of 5 μM for depolarization to −10 mV. In all cases, the test voltage was 300 ms in duration from a holding potential of −80 mV.

Figure 5 shows the tail currents elicited by depolarization to various voltages in the presence of different concentrations of JZTX-XI. In the absence of JZTX-XI, the decay of the tail currents could be well fit by a single exponential function with $\tau \sim 45$ ms when depolarized to −10 mV and was unaffected by the voltage of the preceding depolarization. With weak depolarization to −10 mV, the tail currents that remain in 0.5 μM JZTX-XI have similar kinetics when compared to the control (the deactivation time constants range from 44.7 to 45.8 ms) (Figure 5A,D), while stronger depolarization to +50 and +100 mV results in time constants of 20 and 22.4 ms, respectively. With the concentration of JZTX-XI increased to 5 μM, complete inhibition of currents evoked by weak depolarization (−10 mV) was observed but only partial inhibition for stronger depolarization (+50 or +100 mV). On the other hand, JZTX-XI produces a pronounced speeding of deactivation kinetics, 12.2 and 12.6 ms for depolarization to +50 and +100 mV, respectively (Figure 5B,C,E,F). Faster deactivation kinetics is a characteristic for opening of toxin-bound channels compared to the toxin-unbound channels. The results suggest that currents elicited by strong depolarization in the presence of JZTX-XI are due to the opening of toxin-bound channels.

Effect of JZTX-XI on Nav Channels of Rat DRG Cells and Cardiac Myocytes. Using the whole-cell patch-clamp technique, the actions of JZTX-XI were investigated on Nav channels in rat DRG neurons (TTX-S and TTX-R currents) and cardiac myocytes (mainly TTX-R currents). TTX (200 nM) was added to the external bath solution to separate the TTX-R type from mixture currents. In our experiments on cardiac myocytes, the induced sodium currents were not changed in the absence or presence of TTX at 0.2 μM (data not shown, $n = 4$). Therefore, the effects of JZTX-XI on cardiac myocytes were assayed in bath solution without TTX.

After establishing whole-cell configuration, the experimental cells were held at −80 mV for over 4 min to allow adequate equilibration between the micropipet solution and the cell interior. The current traces were evoked using a 50 ms step depolarization to +50 mV every 2 s. Figure 6A,B

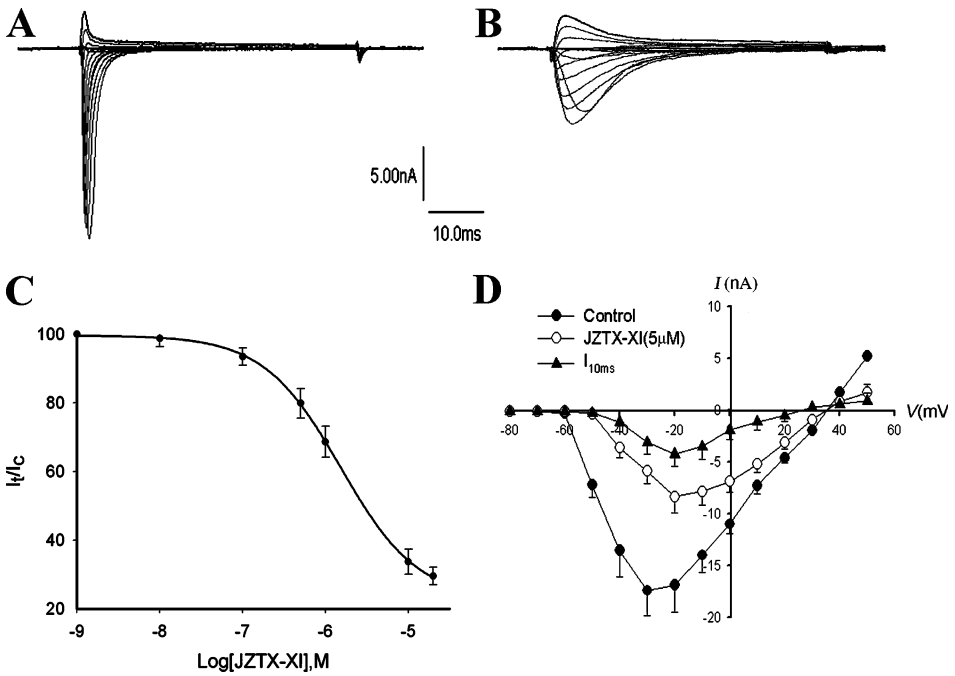

FIGURE 6: Effects of JZTX-XI on Na^+ currents of rat cardiac myocytes. A family of currents was elicited by 50 ms depolarizing steps to various potentials from a holding potential of −80 mV. Test potentials ranged from −80 to +50 mV at increments of +10 mV. (A) Control currents. (B) In the presence of 5 μM JZTX-XI. (C) Concentration-dependent inhibition of Na^+ currents in cardiac myocytes. Every data point (mean ± SEM) coming from three to five cells shows current relative to control. These data points were fitted according to the Boltzmann equation. (D) Effects of JZTX-XI on the current−voltage (I−V) relationship of Na^+ currents in cardiac myocytes. The I−V curve of Na^+ currents showed the relationship between current traces before and after addition of 5 μM JZTX-XI. I_{10ms} was shown as the current inactivated at 10 ms. The data points obtained from four separated experimental cells are shown as the mean ± SEM.

shows the effects in the absence and presence of 5 μM JZTX-XI on Na^+ currents of rat cardiac myocytes, respectively. JZTX-XI was shown to cause a significant reduction in peak Na^+ current amplitude of rat cardiac myocytes with a K_d of 1.28 μM (Figure 6C) and slowing Na^+ current inactivation (Figure 6D). Analysis of the $I-V$ relationship of Na^+ current of rat cardiac myocytes disturbed by 5 μM JZTX-XI (Figure 6D) showed a 10 mV depolarizing shift in the threshold of Nav channel activation whereas no alteration in the reversal potential. JZTX-XI (1 μM) showed no significant effects on the normal activation of both TTX-S and TTX-R Nav currents in DRG neurons (data not shown, $n = 3$).

Effect of JZTX-XI on Cav Channels of Rat DRG Neurons. It is widely accepted that rat DRG cells exhibit two categories of Cav channels: low-voltage-activated (LVA) channels (T-type) and high-voltage-activated (HVA) channels (N, L, P/Q, and R type), which can be discriminated by their voltage dependence and kinetics. Thus, rat DRG cells were chosen for investigating JZTX-XI's effects on Cav channels. No significant inhibition of the HVA and LVA calcium currents in DRG neurons was observed when 1 μM JZTX-XI was applied (data not shown, $n = 3$).

Structure Calculation and Disulfide Determination. Sequence-specific resonance assignments of JZTX-XI were performed via ^{1}H 2D NMR methods following the standard procedures established by Wüthrich (*14*). All of the backbone protons and more than 95% of the side chain protons were identified. The structure of JZTX-XI was determined by using 380 intramolecular distance constraints and 6 dihedral constraints. A family of 20 accepted structures with the lowest energies and the best Ramachandran plots was selected to represent the three-dimensional solution structure of JZTX-XI. A summary of the structural statistics for JZTX-XI is given in Table 1. The structures have no distance violations greater than 0.3 Å and no dihedral violations greater than 3.0°. Analysis of the structures by PROCHECK shows that more than 95% of non-Pro, non-Gly residues lies in the most favored and additionally allowed regions of the Ramachandran plot.

The six Cys residues in JZTX-XI are involved in three disulfide bridges as indicated by mass spectroscopy. The disulfide connection pattern was identified as I−IV, II−V, and III−VI by the observation of inter-cystinyl Hβ_{Cys2}−Hβ_{Cys16}, Hβ_{Cys9}−Hβ_{Cys21}, and Hβ_{Cys15}−Hβ_{Cys28} NOE cross-peaks in the NOESY spectra (200 ms mixing time) of JZTX-XI. This disulfide connection pattern fits the ICK motif, which is frequently found in a variety of toxic and inhibitory peptides from biologically diverse sources (*19*).

Structure Description. A representation of the backbone atoms of the 20 best converged structures of JZTX-XI is shown in Figure 7A. The three-dimensional structure of JZTX-XI (PDB code 2A2V) is composed of two β-strands, strand I (Leu19−Cys21) and strand II (Cys28−Trp30), connected by several reversals. The first chain reversal occurs at residues Lys4−Gly7, which form a type II β-turn. The second and third reversals occur at residues Asp12−Asp14 and Cys16−Leu19, which form a 3_{10}-helical turn and a type IV β-turn (miscellaneous type), respectively. The final reversal occurs at residues Pro23−Lys26 and forms a β-hairpin turn (a type IV β-turn). The cystine knot in JZTX-XI is formed by three disulfide bridges linked as Cys2−Cys16, Cys9−Cys21, and Cys15−Cys28, in which the Cys15−Cys28 disulfide bridge passes through a ring formed by the intervening polypeptide backbone and the Cys2−Cys16 and Cys9−Cys21 disulfide bridges.

Table 1: Structural Statistics for 20 Structures of JZTX-XI (PDB Code 2A2V)

parameter	value
experimental constraints	
intraresidue NOE ($\|i-j\|=0$)	149
sequential NOE ($\|i-j\|=1$)	108
medium-range NOE ($\|i-j\|\leq 5$)	33
long-range NOE ($\|i-j\|\geq 5$)	90
dihedral angle (ϕ)	6
average potential energies (kcal mol^{-1})[a]	
E_{total}	-39.13 ± 4.264
E_{bond}	5.58 ± 0.496
E_{angle}	39.12 ± 1.233
$E_{improper}$	4.57 ± 0.232
E_{vdW}	-92.16 ± 4.378
E_{NOE}	3.73 ± 1.204
E_{cdih}	0.021 ± 0.043
rmsd from experimental constraints[b]	
NOE distance (Å)	0.014 ± 0.002
dihedral angle (deg)	0.139 ± 0.197
rmsd from idealized geometry[a]	
bonds (Å)	0.003 ± 0.0001
angles (deg)	0.535 ± 0.008
impropers (deg)	0.333 ± 0.008
pairwise rms difference of 20 structures (Å)	
backbone atoms (N, Cα, C) (residues 2−30)	0.57 ± 0.12
non-hydrogen heavy atoms (residues 2−30)	1.27 ± 0.15

[a] The statistics of the experimental rms deviation of NOE and dihedral angle constraints were from the calculation with force constants of 50 kcal mol^{-1} Å^{-2} and 200 kcal mol^{-1} rad^{-2}, respectively. [b] The idealized geometry and energy values were defined by the CHARMM force field as implemented in the X-PLOR program. All statistical values of energies, rms deviations, and rms diherences are given as the mean ± SD.

DISCUSSION

A 3.7 kDa peptide toxin named JZTX-XI was isolated from the venom of the tarantula *C. jingzhao* and characterized in this study. JZTX-XI contains 34 residues with the C-terminal residue amidated, which was further verified by its cDNA. The cDNA sequence of JZTX-XI encodes a precursor comprised of a signal peptide, an intervening propeptide, and a mature peptide, suggesting that posttranslational cleavage during secretion is needed for producing mature JZTX-XI. The cDNA structure of JZTX-XI is similar to most other spider cDNA sequences as indicated by GenBank database search. However, JZTX-XI differs from JZTX-I and JZTX-III (*10*, *12*) in their cDNA sequence that the propeptide region length (29 residues) in JZTX-XI is much longer than that (less than 8 residues) of the other two. As the similarities of the pre-propeptide sequences are important criteria for defining the superfamilies for naturally occurring toxins (*16*), the significant difference in the propeptide region of the three jingzhaotoxins implies that, unlike JZTX-I and JZTX-III, JZTX-XI might have come from another progenitor and belong to a different superfamily.

In the two-microelectrode voltage clamp experiments on the Kv channel recorded in *X. laevis* oocytes, JZTX-XI inhibits the Kv2.1 channel with a K_d of 0.74 μM and acts by modulating the voltage dependence of the channel and by inducing a shift in the conductance−voltage relationship

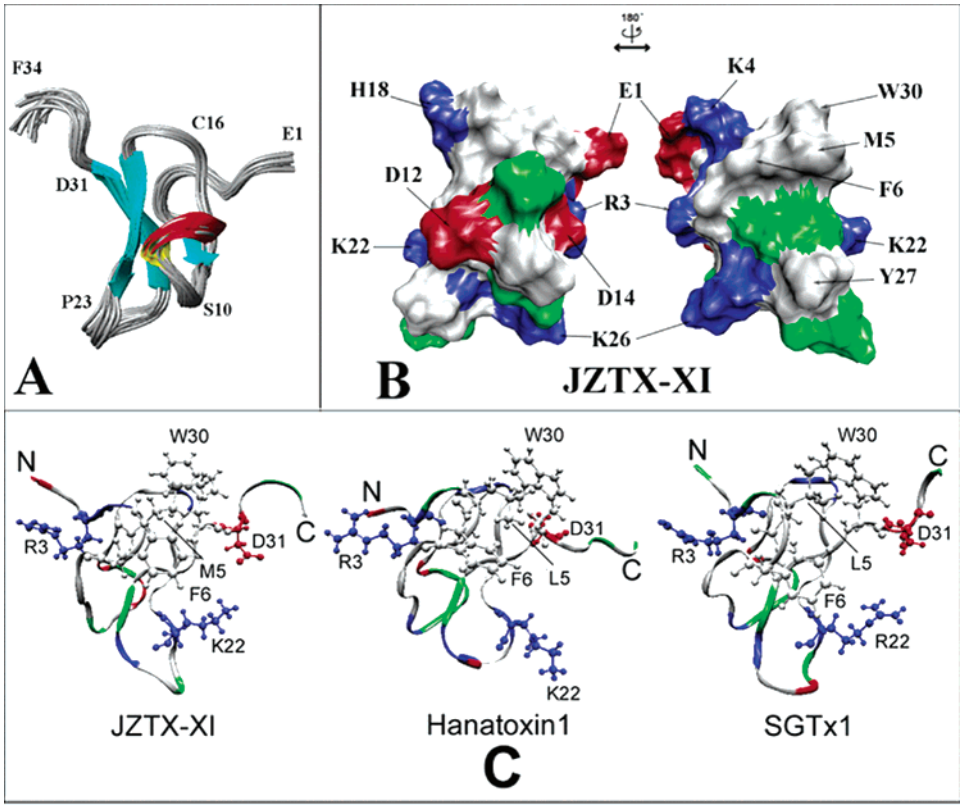

FIGURE 7: Solution structural characterization of JZTX-XI and structural comparison of JZTX-XI with correlated toxin molecules. (A) Ensembles of 20 representative ribbon conformers of the backbone peptide folding of JZTX-XI (PDB code 2A2V). The structure topology of the double-stranded antiparallel β-sheet (cyan) and 3_{10} helical turn (red and yellow) was identified by MOLMOL (*36*). (B) Surface profile of JZTX-XI. The left and right structures are rotated 180° relative to one another about a vertical axis. Hydrophobic residues (Met, Leu, Trp, Ala, Cys, and Tyr) are colored white and basic (Arg and Lys) and acidic (Asp, Glu) residues are colored blue and red, respectively. The other polar residues are colored green. The surface hydrophobic patch residues (Met5, Phe6, and Trp30) and charged residues (Glu1, Arg3, Lys4, Asp12, Asp14, Lys22, Lys26, and Asp31) are indicated. (C) Structural comparison of JZTX-XI to hanatoxin1 (PDB code 1D1H) and SGTx1 (PDB code 1LA4). The surface hydrophobic patches and some interesting charged residues in JZTX-XI, hanatoxin1, and SGTx1 are highlighted and color coded: blue, positively charged; red: negatively charged; white, hydrophobic; green, polar.

to more depolarized potentials (Figure 4). On the other hand, Kv1, Kv3, and Kv4 channels were relatively insensitive to JZTX-XI (Figure 3).

Hanatoxin1 and SGTx1 are two well-known toxins against the Kv2.1 channel, and previous studies (*20*, *21*) have shown that they are channel-gating modifiers with a hydrophobic patch important for their binding to the Kv2.1 channels on their structural surface. In hanatoxin1, this hydrophobic patch is mainly comprised of L5, F6, and W30 (Figure 7C); around this patch there allocates many highly polar residues, including six basic residues (R3, K10, K26, R24, K22, and K17) and four acidic residues (E1, D25, D31, and D14), the protrudent hydrophobic patch, and some of these surrounded charged residues might be important for interacting with the C-terminus of the S3 segment within the voltage-sensor paddle of the Kv2.1 channel (*22*, *23*). Similarly, mutational scanning studies of SGTx1 (*24*), a Kv2.1 channel inhibitor sharing high structural and functional similarity with hanatoxin1, suggest that three hydrophobic residues (L5, F6, W30) and two basic residues (R3, R22) are involved in the binding. On the basis of these studies, it seems likely that I273 and F274 of the Kv2.1 channel interact with the hydrophobic surface of hanatoxin1 or SGTx1, while E277 interacts with basic residues surrounding this hydrophobic patch. Structural comparison with hanatoxin1 and SGTx1 reveals that JZTX-XI adopts a similar surface profile comprised of a hydrophobic patch (M5, F6, and W30) and several charged residues (R3, K22, and D31) around it (Figure 7B). Sequence alignments of the three toxins indicate that R3, F6, K26, and W30 are strictly conserved positions, whereas M5 and K22 in JZTX-XI are also conservatively replaced by L5 and R22 in SGTx1 (L5 for hanatoxin1) (Figure 7C), respectively. These results clearly indicate an action manner of JZTX-XI similar to that of hanatoxin1 and SGTx1.

The selectivity of many gating-modifier spider toxins is promiscuous within or across voltage-gated ion channel families. For example, ScTx1 inhibits Kv2.1, Kv2.2, and Kv4.2 channels (*25*); hanatoxin1 and grammotoxin inhibit both Kv2.1 channels and Cav2.1 channels (*26*); ProTx-I inhibits Nav, Gav, and Kv channels (*27*). Such promiscuous activity was also found in present study when we tested the activity of JZTX-XI against Nav and Cav channels via patch-clamp experiments. JZTX-XI showed a capability of modulating gating in Nav channels of rat cardiac myocyte and failed to affect the Nav and Cav channels in rat DRG neurons. In the electrophysiological experiments on rat cardiac Nav channels, JZTX-XI caused a slowing of voltage-gated Na^+ current inactivation and a significant reduction in peak Na^+ current (K_d 1.28 μM) with a threshold shift of 10 mV in the depolarizing direction (Figure 6). To rule out the possibility that a very potent minor contaminant was present, we have taken great care to ensure that the results were obtained with purified toxins. By three metrics (MS,

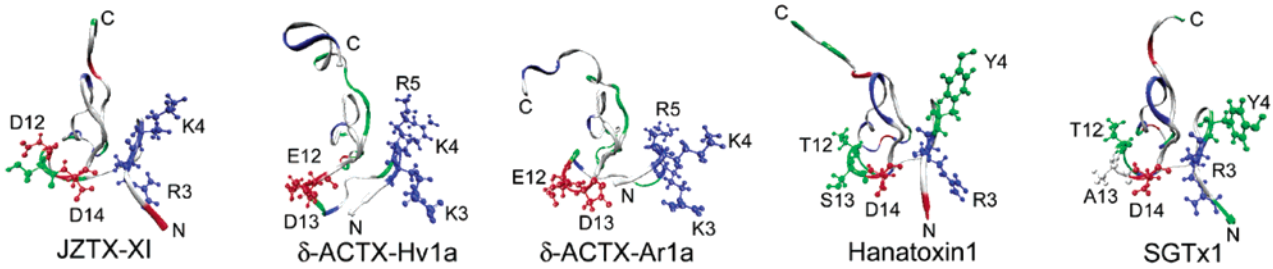

FIGURE 8: Structural comparison of JZTX-XI with δ-ACTX-Hv1a (PDB code 1VTX), δ-ACTX-Ar1a (PDB code 1QDP), hanatoxin1, and SGTx1. Topologically related residues in these toxins are highlighted, and the color code is the same as in Figure 7C.

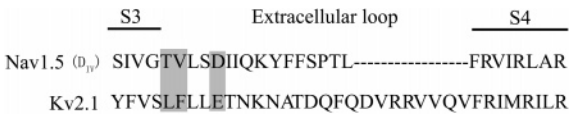

FIGURE 9: Analysis of amino acid sequences of the S3−S4 linker on Nav1.5 (domain IV) and Kv2.1 channels. The emerging positions of functional residues are shaded in gray.

protein sequencing, and HPLC analysis), the purity of native JZTX-XI was estimated to be >99%.

Gating modifiers of Nav channels can be classified into two groups: excitatory toxins and depressant toxins according to their distinct pharmacological characterization (*7*). For example, α-scorpion toxins are typical excitatory toxins that bind to the channel in a voltage-dependent manner and cause a marked slowing of inactivation (*28*, *29*). On the other hand, *β*-scorpion toxins produce a negative shift of the Na^+ conductance and decrease the peak current, without affecting the rate of inactivation (*30*). We had isolated and characterized two toxins, JZTX-I and JZTX-III, from the venom of *C. jingzhao* in previous work. These two toxins preferentially interacted with Nav channels of rat cardiac myocytes with a mechanism similar to that of α- and *β*-type scorpion toxins, respectively (*10*, *12*). However, the effect of JZTX-XI does not conform to either a typical α- or *β*-type activity but is similar to that of *δ*-ACTX, such as *δ*-ACTX-Hv1a and *δ*-ACTX-Ar1a from the venom of the Blue Mountains funnel-web spider *Hadronyche versuta* (*31*−*33*), both of which have a pronounced effect on Nav channel inactivation and reduce the peak Na^+ currents.

The promiscuous activity of JZTX-XI on both Kv2.1 and Nav1.5 channels raises concerns of how conserved the binding domains are in these two channels. The S3−S4 linker of voltage-gating ion channels was thought to be a hot spot that many gating modifiers, such as hanatoxin1, grammotoxin, α-scorpion toxins, and sea anemone toxins, bind to (*26*, *28*). An alignment of this region (Figure 9) between Nav1.5 and Kv2.1 channels shows that residues T1609, V1610, and D1613 on domain IV of the Nav1.5 channel correspond to the L273, F274, and E277 of the Kv2.1 channel, which might be crucial for the binding affinity of both hanatoxin1 (*18*) and grammotoxin (*26*). The above comparison together with the structural and functional similarity between JZTX-XI and hanatoxin1 implies that similar to the toxin−channel recognition of hanatoxin1 on Kv2.1 and Cav2.1, JZTX-XI might interact with the same region of the Kv2.1 and Nav1.5 channels.

On the other hand, previous studies proposed that K3, R5, and D13 of *δ*-ACTX are critical residues involved in the binding of toxin to site 3 of the Nav channel (*34*, *35*). An action manner on Nav channels of JZTX-XI similar to that of *δ*-ACTX was observed in our experiments, which implies that JZTX-XI might bind to Nav channels with an active site different from that of hanatoxin1 binding. Structural comparison of JZTX-XI, *δ*-ACTX-Hv1a, and *δ*-ACTX-Ar1a shows that, in JZTX-XI, the conserved positively and negatively charged residues R3, K4, D12, and D14 form a bioactive surface similar to that of *δ*-ACTX, whereas K4 and D12 of JZTX-XI are replaced by Y4 and T12 in hanatoxin1 and SGTx1, respectively (Figure 8). The topologic similarity of these charged residues between JZTX-XI and *δ*-ACTX may explain their similar action manner on Nav channels. However, further mutant studies are needed to clarify the role of each residue involved in toxin−channel binding.

In summary, JZTX-XI is a novel toxin that specifically modifies the gating of both the Kv2.1 and Nav1.5 channel. The structure and function study of this toxin paves a way for further detailed analysis of how this toxin interacts with various ion channels. Moreover, as a toxin targeting Nav channels of cardiac myocytes rather than DRG neurons, JZTX-XI might be an ideal tool for analysis of the Nav channels on cardiac myocytes and for pharmacologic exploitation on cardiac-related disease.

ACKNOWLEDGMENT

We are grateful to Guangzhong Tu of Beijing Institute of Microchemistry for collecting the ^1H NMR spectra. We thank Professor Sylvie Diochot (Pharmacien, Ingenieur de Recherche au CNRS) for providing the Kv2.1, Kv1.1, and Kv4.1 clones. The Kv1.2 clone was kindly provided by Lily Jan. We are grateful to Maria L. Garcia (Merck) for providing the Kv1.3 clone. We thank Stanley Nattel for providing the Kv1.4 and Kv3.1 clones. We also thank Jeanne M. Nerbonne for providing the Kv4.2 clone and Martin Stocker for another Kv2.1 clone.

REFERENCES

1. Shieh, C. C., Coghlan, M., Sullivan, J. P., and Gopalakrishnan, M. (2000) Potassium channels: molecular defects, diseases, and therapeutic opportunities, *Pharmacol. Rev. 52*, 557−594.
2. Jiang, Y., Lee, A., Chen, J., Ruta, V., Cadene, M., Chait, B. T., and MacKinnon, R. (2003) The principle of gating charge movement in a voltage-dependent K^+ channel, *Nature 423*, 33−41.
3. Jiang, Y., Ruta, V., Chen, J., Lee, A., and MacKinnon, R. (2003) The principle of gating charge movement in a voltage-dependent K^+ channel, *Nature 423*, 42−48.
4. Lu, Z., Klem, A. M., and Ramu, T. (2001) Coupling between voltage sensors and activation gate in voltage-gated K^+ channels, *Nature 413*, 809−813.
5. Catterall, W. A. (1996) Molecular properties of sodium and calcium channels, *J. Bioenerg. Biomembr. 28*, 219−230.

6. Xiao, Y. C., and Liang, S. P. (2003) Inhibition of sodium channels in rat dorsal root ganglion neurons by hainantoxin-IV, a novel spider toxin, *Sheng Wu Hua Xue Yu Sheng Wu Wu Li Xue Bao (Shanghai)*, *35*, 82−85.
7. Li, D., Xiao, Y., Hu, W., Xie, J., Bosmans, F., Tytgat, J., and Liang, S. (2003) Function and solution structure of hainantoxin-I, a novel insect sodium channel inhibitor from the Chinese bird spider, *Selenocosmia hainana. 18*, *555*, 616−622.
8. Swartz, K. J., and MacKinnon, R. (1995) An inhibitor of the Kv2.1 potassium channel isolated from the venom of a Chilean tarantula, *Neuron 15*, 941−949.
9. Mintz, I. M., Venema, V. J., Swiderek, K. M., Lee, T. D., Bean, B. P., and Adams, M. E. (1992) P-type calcium channels blocked by the spider toxin w-Aga-IVA, *Nature 355*, 46−52.
10. Xiao, Y., Tang, J., Yang, Y., Wang, M., Hu, W., Xie, J., Zeng, X., and Liang, S. (2004) Jingzhaotoxin-III, a novel spider toxin inhibiting activation of voltage-gated sodium channel in rat cardiac myocytes, *J. Biol. Chem. 279*, 26220−26226.
11. Salinas, M., Duprat, F., Heurteaux, C., Hugnot, J. P., and Lazdunski, M. (1997) New modulatory alpha subunits for mammalian shab K^+ channels, *J. Biol. Chem. 272*, 24371−24379.
12. Yucheng, X., Jianzhou, T., Weijun, H., Chantal, M., Jan, T., and Songping, L. (2005) Jingzhaotoxin-I, a novel spider neurotoxin preferentially inhibiting cardiac sodium channel inactivation, *J. Biol. Chem.*, *280*, 12069−12076.
13. Cao, C. M., Xia, Q., Chen, Y. Y., Zhang, X., and Shen, Y. L. (2002) Opioid receptor-mediated effects of interleukin-2 on the $[Ca^{2+}]$ transient and contraction in isolated ventricular myocytes of the rat. *Pfluegers Arch. Eur. J. Physiol. 443*, 635−642.
14. Wüthrich, K. (1986) *NMR of Proteins and Nucleic Acids*, Wiley, New York.
15. Schwieters, C. D., Kuszewski, J. J., Tjandra, N., and Clore, G. M. (2003) The X-PLOR-NIH NMR molecular structure determination package, *J. Magn. Reson. 160*, 66−74.
16. Diao, J. B., Lin, Y., Tang, J. Z., and Liang, S. P. (2003) cDNA sequence analysis of seven peptide toxins from the spider *Selenocosmia huwena*, *Toxicon 42*, 715−723.
17. Lee, S.-Y., and MacKinnon, R. (2004) A membrane-access mechanism of ion channel inhibition by voltage sensor toxins from spider venom, *Nature 430*, 2232−2235.
18. Swartz, K. J., and MacKinnon, R. (1997) Hanatoxin modifies the gating of a voltage-dependent K1 channel through multiple binding sites, *Neuron 18*, 675−682.
19. Pallaghy, P. K., Nielsen, K. J., Craik, D. J., and Norton, R. S. (1994) A common structural motif incorporating a cystine knot and a triple-stranded beta-sheet in toxic and inhibitory polypeptides, *Protein Sci. 3*, 1833−1839.
20. Takahashi, H., Kim, J. I., Min, H. J., Sato, K., Swartz, K. J., and Shimada, I. (2000) Solution structure of hanatoxin1, a gating modifier of voltage-dependent K^+ channels: common surface features of gating modifier toxins, *J. Mol. Biol. 297*, 771−780.
21. Lee, C. W., Kim, S., Roh, S. H., Endoh, H., Kodera, Y., Maeda, T., Kohno, T., Wang, J. M., Swartz, K. J, and Kim, J. I. (2004) Solution structure and functional characterization of SGTx1, a modifier of Kv2.1 channel gating, *Biochemistry 43*, 890−897.
22. Li-Smerin, Y., and Swartz, K. J. (2000) Localization and molecular determinants of the hanatoxin receptors on the voltage-sensing domains of a K^+ channel, *J. Gen. Physiol. 115*, 673−684.
23. Li-Smerin, Y., and Swartz, K. J. (2001) Helical structure of the COOH terminus of S3 and its contribution to the gating modifier toxin receptor in voltage-gated ion channels, *J. Gen. Physiol. 117*, 205−218.
24. Wang, J. M., Roh, S. H., Kim, S., Lee, C. W., Kim, J. I., and Swartz, K. J. (2004) Molecular surface of tarantula toxin interacting with voltage sensors in Kv channels, *J. Gen. Physiol. 123*, 455−467.
25. Escoubas, P., Diochot, S., Celerier, M. L., Nakajima, T., and Lazdunski, M. (2002) Novel tarantula toxins for subtypes of voltage-dependent potassium channels in the Kv2 and Kv4 subfamilies, *Mol. Pharmacol. 62*, 48−57.
26. Li-Smerin, Y., and Swartz, K. J. (1998) Gating modifier toxins reveal a conserved structural motif in voltage-gated Ca^{2+} and K^+ channels, *Proc. Natl. Acad. Sci. U.S.A. 95*, 8585−8589.
27. Richard, E. M., Vivien, A. W., Richard, L. K., Jeremy, C. H., Chou, J. L., Ge, Dai., Richard, M. B., Martin, G. K., Ying-Duo, Gao., Victor, M. G., Michael, J. B., John, T. M., Charles, J. C., and McHardy, M. S. (2002) Two tarantula peptides inhibit activation of multiple sodium channels, *Biochemistry 41*, 14734−14747.
28. Rogers, J. C., Qu, Y., Tanada, T. N., Scheuer, T., and Catterall, W. A. (1996) Molecular determinants of high affinity binding of α-scorpion toxin and sea anemone toxin in the S3-S4 extracellular loop in domain IV of the Na^+ channel R subunit, *J. Biol. Chem. 271*, 15950−15962.
29. Sheets, M. F., and Hanck, D. A. (1995) Voltage-dependent open-state inactivation of cardiac sodium channels: gating current studies with anthopleurin-a toxin, *J. Gen. Physiol. 106*, 617−640.
30. Cestele, S., Qu, Y., Rogers, J. C., Rochat, H., Scheuer, T., and Catterall, W. A. (1998) Voltage sensor-trapping: enhanced activation of sodium channels by β-scorpion toxin bound to the S3-S4 loop in domain II, *Neuron 21*, 919−931.
31. Nicholson, G. M., Willow, M., Howden, M. E., and Narahashi, T. (1994) Modification of sodium channel gating and kinetics by versutoxin from the Australian funnel-web spider *Hadronyche versuta*, *Pfluegers Arch. 428*, 400−409.
32. Nicholson, G. M., Walsh, R., Little, M. J., and Tyler, M. I. (1998) Characterisation of the effects of robustoxin, the lethal neurotoxin from the Sydney funnel-web spider *Atrax robustus*, on sodium channel activation and inactivation, *Pfluegers Arch. 436*, 117−126.
33. Szeto, T. H., Birinyi-Strachan, L. C., Smith, R., Connor, M., Christie, M. J., King, G. F., and Nicholson, G. M. (2000) Isolation and pharmacological characterisation of delta-atracotoxin-Hv1b, a vertebrate-selective sodium channel toxin, *FEBS Lett. 470*, 293−299.
34. Fletcher, J. I., Chapman, B. E., Mackay, J. P., Howden, M. E., and King, G. F. (1997) The structure of versutoxin (delta-atracotoxin-Hv1) provides insights into the binding of site 3 neurotoxins to the voltage-gated sodium channel, *Structure 5*, 1525−1535.
35. Gilles, N., Harrison, G., Karbat, I., Gurevitz, M., Nicholson, G. M., and Gordon, D. (2002) Variations in receptor site-3 on rat brain and insect sodium channels highlighted by binding of a funnel-web spider delta-atracotoxin, *Eur. J. Biochem. 269*, 1500−1510.
36. Koradi, R., Billeter, M., and Wüthrich, K. (1996) MOLMOL: a program for display and analysis of macromolecular structures, *J. Mol. Graphics 14*, 51−55..

BI061457+